Simulation of Five-Step One-Bed Sorption-Enhanced Reaction Process

Guo-hua Xiu, Jose Luciano Soares, Ping Li, and Alirio E. Rodrigues
Laboratory of Separation and Reaction Engineering, Faculty of Engineering, University of Porto, s/n, 4200-465 Porto, Portugal
and
Dept. of Chemical Engineering, Shenyang Institute of Chemical Technology, Shenyang 110021, P. R. China

A five-step, one-bed, sorption-enhanced reaction process proposed by Carvill et al. in 1996 for hydrogen production by steam–methane reforming was analyzed. For the simulated results of the first step, data from Hufton et al. (1999) and Ding and Alpay (2000) for a fixed-bed column of an admixture of a catalyst and a sorbent that selectively removes CO_2 from the reaction zone were used. The sorbent is periodically regenerated by using the principles of pressure-swing adsorption. The process steps allow direct production of hydrogen with high purity and high methane conversion. A model considering multicomponent and overall mass balance, Ergun relation for pressure drop, energy balance for the bed-volume element, and nonlinear adsorption equilibrium isotherm coupled with three main reactions was derived to describe the sorption-enhanced reaction cyclic process. Two different isotherms were used under wet and dry conditions. The LDF model adopted describes the mass-transfer rate of CO_2 in the adsorbent. Numerical solution of model equations for the cyclic process was obtained by the orthogonal collocation method. The operating conditions allow the combination of a sufficiently high purity of hydrogen (average purity over 80%) with traces of CO and CO_2, high methane conversion, fast adsorbent regeneration, and cyclic steady-state operation. The model predictions agree reasonably with the literature data. The package is suitable for the design and analysis of sorption-enhanced reaction process.

Introduction

Hydrogen is used extensively by many industries for a variety of applications; it is produced industrially by several methods, such as steam reforming, electrolysis of water, ammonia dissociation, and partial oxidation. In addition, hydrogen is obtained as a byproduct of some refining and chemical production processes. Manufacture via steam reforming of natural gas is a low-cost option for hydrogen production (Ridler and Twigg, 1989).

Many reactions are limited by equilibrium, and the production of hydrogen by steam–methane reforming is a good example. The combination of reaction and separation in a single unit operation has advantages for achieving enhanced conversions and yields in catalyzed reversible reactions; this concept is based on the well-known Le Chatelier's principle that (1) the conversion of reactants to products, and (2) the rate of forward reaction in an equilibrium-limited reaction can be increased by selectively removing some of the reaction products from the reaction zone (Gluud et al., 1931).

Configurations under investigation include selective adsorption with reaction (Roginskii et al., 1962; Magee, 1963; Chu and Tsang, 1971; Takeuchi and Uraguchi, 1977; Cho et

Correspondence concerning this article should be addressed to A. E. Rodrigues.
Current address of J. L. Soares: Dept. of Chemical Engineering, Federal University of Santa Catarina, PO Box 476, CEP 88040-900, Florianopolis, SC, Brazil.

al., 1980, 1982; Petroulas et al., 1985; Fish et al., 1986; Tonkovich and Carr, 1994a,b; Kruglov, 1994; Lu and Rodrigues, 1994; Carvill et al., 1996; Hufton et al., 1999, 2000; Ding and Alpay, 2000b), selective permeation with reaction (Sun and Khang, 1988; Hsieh, 1989; Champagnie et al., 1990; Wu et al., 1990; Uemiya et al., 1991; Tsotsis et al., 1992; Itoh et al., 1993; Adris et al., 1994; Armor, 1995; Balachandran et al., 1997; Omorjan et al., 1999; Ostrowski and Mleczko, 1999), and imposed thermal effects (Rostrup-Nielsen, 1993; Jachuck and Ramshaw, 1994; Matros and Bunimovich, 1995; Salinger and Eigenberger, 1996; Yongsunthon and Alpay, 1998, 1999). Of particular interest is a pressure swing adsorptive (PSA) reactor.

If an adsorbent selectively trapping the product is combined with the catalyst, conversion can almost run to completion. The PSA reactor, in which a high-pressure feed of synthesis gas to a mixed bed of adsorbent and catalyst (reaction and adsorption of CO_2) is combined with rapid pressure release to low pressure (CO_2 desorption), is one reasonable configuration for such a production process (Carvill et al., 1996; Hufton et al., 1999, 2000; Ding and Alpay, 2000b).

From the point of view of application, two key problems should be solved for hydrogen production by sorption-enhanced steam–methane reforming process: (1) to find suitable adsorbent with high adsorption capacity, high mass-transfer rates for both adsorption and desorption of CO_2 for its removal from the reaction zone, and regeneration; (2) to seek out a simplistic and energy-saving cyclic process for adsorbent regeneration. Because of the high complexity of the process, the design and optimization of the PSA reactor based only on experiments is not possible.

There are a large number of adsorbents for CO_2 removal, which include various metal oxides (e.g., CaO, MgO), alumina and metal-promoted alumina, activated carbon, and zeolites (e.g., 4A, 5A, CrA, CrX, CrY, RhA, 13X, and Na- and H-mordenites) (Ma and Mancel, 1972; Ma and Roux, 1973; Hayhurst, 1980; Wilson and Danner, 1983; Valenzuela and Myers, 1989; Han and Harrison, 1994; Anand et al., 1995; Hufton et al., 1999; Ding and Alpay, 2000a).

The stability of the adsorbent under cyclic reactor conditions, that is, under constant temporal and spatial variations of gas composition and temperature, will govern the commercial feasibility. Most recently CO_2 adsorption capacity on hydrotalcite has been presented (Hufton et al., 1999; Ding and Alpay, 2000a). Hydrotalcite is an anionic clay consisting of positively charged layers of metal oxide (or metal hydroxide) with interlayers of anions, such as carbonate. Exchange of the metal cations, as well as intercalation of the anionic layer can lead to a wide range of catalytic and adsorptive properties, with particular stability under wet gas and high-temperature conditions (Hufton et al., 1999; Ding and Alpay, 2000a). Thus, such materials are potentially suitable for the separation-enhanced steam–methane reforming process, and these types of adsorbents are commercially available now (see Zou et al., 2001).

A two-, three-, four-, or five-step simplistic process is considered by most of the published works theoretically and experimentally. Kadlec and coworkers experimentally (Vaporciyan and Kadlec, 1989) and theoretically (Vaporciyan and Kadlec, 1987; Lee and Kadlec, 1989) evaluated a three-step process consisting of (1) introduction of the reactant–feedgas mixture into a packed bed of catalyst and adsorbent at an elevated pressure for a short period of time, followed by (2) a short delay period when the introduction of feedgas was stopped, and finally (3) countercurrent depressurization of the packed bed to the lowest pressure level of operation.

Alpay and coworkers (Alpay et al., 1993, 1994; Chatsiriwech et al., 1994; Kirkby and Morgan, 1994; Ding and Alpay, 2000b) evaluated model solutions of the PSA reactor system using a process similar to that just mentioned except where step (2) was eliminated (Alpay et al., 1993). They also theoretically evaluated a four-step process (Alpay et al., 1994; Chatsiriwech et al., 1994; Kirkby and Morgan, 1994) consisting of (1) pressurizing the packed bed of catalyst and adsorbent with the reactant-feed mixture to a higher pressure level, (2) feeding the reactant mixture at the elevated pressure and withdrawing a product gas, (3) countercurrently depressurizing the reactor to the lowest pressure level of operation, and (4) countercurrently purging the reactor with the effluent from step 2. A variation of this cycle included partial countercurrent pressurization of the reactor with the effluent from step 2 before step 1 started (Kirkby and Morgan, 1994).

Sircar and coworkers (Carvill et al., 1996) considered a general equilibrium-controlled reaction involving one or more reactants producing a desired reaction product and a byproduct. They proposed a five-step one-bed process, and used the reverse water–gas shift reaction to produce high-purity CO as an example. They applied this concept to hydrogen production by the steam–methane reforming process (Hufton et al., 1999), and later improved the process cycle suggesting a four-step one-bed process for hydrogen production (Hufton et al., 2000).

In this article, a five-step (high-pressure reaction/adsorption, depressurization, low-pressure purge with methane, low-pressure purge with part of hydrogen product, and pressurization with part of hydrogen product) one-bed sorption-enhanced reaction process (proposed by Carvill et al., 1996) was theoretically analyzed for hydrogen production by steam–methane reforming. The simulated data for the first step use data from the articles of Hufton et al. (1999) and Ding and Alpay (2000a,b). A model that takes into account multicomponent (six species) mass balances, overall mass balance, Ergun relation (Ergun, 1952) for pressure drop, energy balance for bed-volume element including the heat-transfer to the column wall, and nonlinear adsorption equilibrium isotherm coupled with the three main reactions was derived to describe the sorption-enhanced reaction cyclic process. Two different isotherms were used under wet and dry conditions; the linear driving-force (LDF) model was adopted to describe the mass-transfer rate of CO_2 to the adsorbent. A numerical solution of the model equations for the cyclic process was obtained by using the method of orthogonal collocation (Malek and Farooq, 1997). The purpose of this work is to find suitable operating conditions that allow the production of a sufficiently high hydrogen purity (average purity over 80%) with traces of CO and CO_2, high methane conversion, fast adsorbent regeneration, and cyclic steady-state operation.

Process Description

The operation scheme of the five-step one-bed sorption-enhanced reaction process is shown in Figure 1. The three

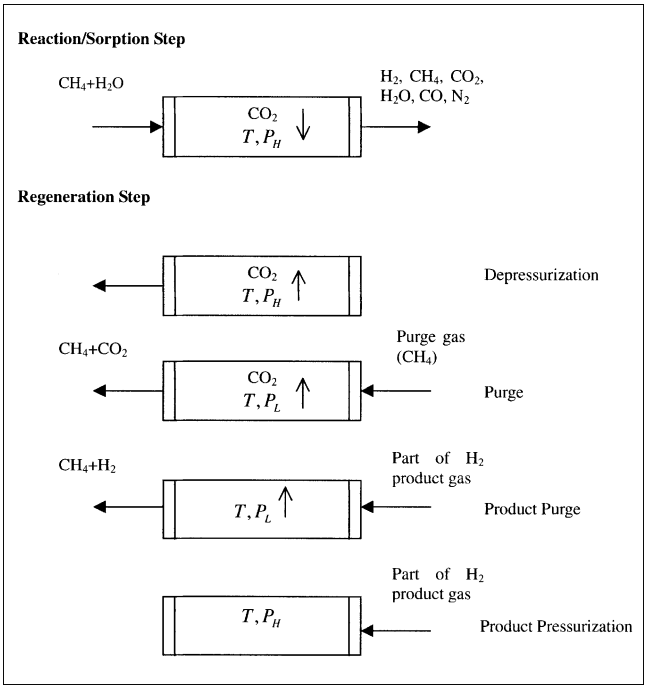

Figure 1. Flow direction for five-step one-bed sorption-enhanced reaction process.

↓ means adsorption; ↑ means desorption.

main chemical reactions in the cycle are described by Eq. 1 (Xu and Froment, 1989)

$$\begin{cases} CH_4 + H_2O \Leftrightarrow CO + 3H_2,\ \Delta H_{298} = 206.2\ \text{kJ/mol (I)} \\ CH_4 + 2H_2O \Leftrightarrow CO_2 + 4H_2,\ \Delta H_{298} = 164.9\ \text{kJ/mol (II)} \\ CO + H_2O \Leftrightarrow CO_2 + H_2,\ \Delta H_{298} = -41.1\ \text{kJ/mol (III)} \end{cases} \quad (1)$$

Only two of the three reactions are linearly independent. The reaction kinetic model of Xu and Froment (1989) can be summarized as

$$R_I = \frac{1}{(DEN)^2}\frac{k_1}{P_{H_2}^{2.5}}\left(P_{CH_4}P_{H_2O} - \frac{P_{H_2}^3 P_{CO}}{K_I}\right) \quad (1a)$$

$$R_{II} = \frac{1}{(DEN)^2}\frac{k_2}{P_{H_2}^{3.5}}\left(P_{CH_4}P_{H_2O}^2 - \frac{P_{H_2}^4 P_{CO_2}}{K_{II}}\right) \quad (1b)$$

$$R_{III} = \frac{1}{(DEN)^2}\frac{k_3}{P_{H_2}}\left(P_{CO}P_{H_2O} - \frac{P_{H_2}P_{CO_2}}{K_{III}}\right), \quad (1c)$$

where $DEN = 1 + K_{CO}P_{CO} + K_{H_2}P_{H_2} + K_{CH_4}P_{CH_4} + K_{H_2O}P_{H_2O}/P_{H_2}$, in which $P_i = y_i P$ ($i = H_2O$, CH_4, H_2, CO_2, and CO, P is the local total pressure, and y_i is the gas-phase mole fraction of component i). For the expressions of k_1, k_2, k_3, K_{CO}, K_{H_2}, K_{CH_4} and K_{H_2O} and K_I, K_{II} and K_{III}, see Table 1.

The equilibrium data K_I, K_{II}, and K_{III} are the key parameters for our simulation. There are two sources (Xu and Froment, 1989; Twigg, 1989) from which to obtain their expressions, as listed in Table 1; for our work, we take the results of Twigg (1989).

The formation or consumption rate of component i, r_i, was then calculated by using Eqs. 1a–1c as follows:

$$r_i = \sum_{j=I}^{III} \upsilon_{ij} R_j \ (i = CH_4, H_2O, H_2, CO_2, CO), \quad (2a)$$

where υ_{ij} is the stoichiometric coefficient of component i in reaction j. If i refers to a reactant, υ_{ij} is negative, and for a

Table 1. Parameters Used in Eq. 1

$$K_I = \frac{1}{\exp(0.2513Z^4 - 0.3665Z^3 - 0.58101Z^2 + 27.1337Z - 3.2770)}\ \text{atm}^2,^*\ K_{II} = K_I K_{III}$$

$$K_{III} = \exp(-0.29353Z^3 + 0.63508Z^2 + 4.1778Z + 0.31688),^{**}\ \text{where } Z = \frac{1{,}000}{T} - 1$$

$$k_1 = 1.842\times10^{-4}\exp\left[-\frac{240{,}100}{R}\left(\frac{1}{T} - \frac{1}{648}\right)\right]\ \text{kmol}\cdot\text{bar}^{0.5}/\text{kg}_{cat}\cdot\text{h}$$

$$k_2 = 2.193\times10^{-5}\exp\left[-\frac{243{,}900}{R}\left(\frac{1}{T} - \frac{1}{648}\right)\right]\ \text{kmol}\cdot\text{bar}^{0.5}/\text{kg}_{cat}\cdot\text{h}$$

$$k_3 = 7.558\exp\left[-\frac{67{,}130}{R}\left(\frac{1}{T} - \frac{1}{648}\right)\right]\ \text{kmol}/\text{kg}_{cat}\cdot\text{h}\cdot\text{bar}$$

$$K_{CH_4} = 0.179\exp\left[\frac{38{,}280}{R}\left(\frac{1}{T} - \frac{1}{823}\right)\right]\ \text{bar}^{-1}, \qquad K_{H_2O} = 0.4152\exp\left[-\frac{88{,}680}{R}\left(\frac{1}{T} - \frac{1}{823}\right)\right]$$

$$K_{CO} = 40.91\exp\left[\frac{70{,}650}{R}\left(\frac{1}{T} - \frac{1}{648}\right)\right]\ \text{bar}^{-1}, \qquad K_{H_2} = 0.0296\exp\left[\frac{82{,}900}{R}\left(\frac{1}{T} - \frac{1}{648}\right)\right]\ \text{bar}^{-1}$$

Source: Xu and Froment, 1989; Twigg, 1989.

*, ** are taken from Twigg (1989). The data of Xu and Froment (1989) are as follows: $K_I = 4.707\times10^{12}\exp\left(-\frac{224{,}000}{RT}\right)\ \text{bar}^2$, $K_{III} = 1.142\times10^{-2}\exp\left(\frac{37{,}300}{RT}\right)$ (for $T = 948$ K).

product v_{ij} is positive. Thus, we have

$$r_{CH_4} = -R_I - R_{II} \tag{2b}$$

$$r_{H_2O} = -R_I - 2R_{II} - R_{III} \tag{2c}$$

$$r_{H_2} = 3R_I + 4R_{II} + R_{III} \tag{2d}$$

$$r_{CO} = R_I - R_{III} \tag{2e}$$

$$r_{CO_2} = R_{II} + R_{III}. \tag{2f}$$

Reforming reactions (I) and (II) are strongly endothermic, so the forward reaction is favored by high temperatures, while the water–gas shift reaction (III) is moderately exothermic and is therefore favored by low temperatures. The reforming reactions will also be favored at low pressures, whereas the water–gas shift reaction is largely unaffected by changes in pressure. In the presence of a selective CO_2 adsorbent, the conversion of CH_4 to CO_2 is favored. For a reaction that is not kinetically limited, the use of an adsorbent will thus enable a lower operating temperature for a desired conversion. However, the separation effect is lost on equilibrium of the adsorbent. This is why the periodic regeneration of the adsorbent is needed.

The five steps of a one-bed sorption-enhanced reaction process are described below (Carvill et al., 1996) for our case.

Step 1: High-Pressure Reaction/Adsorption. Feed a stoichiometric mixture of H_2O and CH_4 at high pressure P_H through the regenerated reactor that has been previously saturated with part of the H_2 product gas at P_H. An effluent stream containing essentially H_2 is produced from the reactor at pressure P_H. The step is continued until near breakthrough point of CO_2.

Step 2: Countercurrent Blowdown Step. Depressurize the reactor to a lower pressure level of P_L countercurrent to that of the reactant–feed-gas flow. A gas stream containing all the components of the system exits the reactor. This stream consists of interparticle void gas in the column as well as some adsorbed gases present in the reactor at the end of Step 1. The reaction and desorption of CO_2 should take place in the countercurrent blowdown step.

Step 3: Low-Pressure Purge with Methane. Introduce methane to the reactor at P_L in the direction countercurrent to that of the reactant feedgas flow. This step desorbs most of the remaining adsorbed CO_2, and the reactor effluent gas contains a mixture of CH_4 and CO_2. The reactor is essentially saturated with CH_4 at P_L at the end of this step.

Step 4: Low-Pressure Purge with Part of the Hydrogen Product Gas. Purge the reactor countercurrently at P_L with H_2 in order to remove CH_4 from the reactor void space and further desorb CO_2 from the adsorbent. After two purge steps, the adsorbent is regenerated, and the remaining carbon dioxide concentration in the fixed-bed reactor is low enough for the next cycle.

Step 5: Countercurrent Repressurization with Part of Hydrogen Product. Pressurize the reactor from P_L to P_H by countercurrently introducing part of the H_2 product gas from Step 1. During the countercurrent repressurization step, a part of the

Table 2. Parameters for Governing Equations

Semi-empirical relationships for K_D and K_V (Ergun, 1952):

$$K_D = \frac{150\mu(1-\epsilon_b)^2}{d_p^2\epsilon_b^3}(\mathrm{N\cdot s/m^4}),\ K_V = \frac{1.75(1-\epsilon_b)}{d_p\epsilon_b^3}\frac{PM}{RT}(\mathrm{N\cdot s^2/m^5}),\ \text{in which } M \approx 0.018\ \mathrm{kg/mol}$$

Axial dispersion coefficient D_L (Edwards and Richardson, 1968)

$$D_L = 0.73D_m + \frac{0.5ud_p}{1+9.49D_m/(ud_p)}(\mathrm{m^2/s}),\ \text{in which } D_m = 1.6\times10^{-5}\ \mathrm{m^2/s} \text{ for } P_H \text{ and } T_f, \text{ and}$$

$D_m = 5.6\times10^{-5}\ \mathrm{m^2/s}$ for P_L and T_f (Reid et al., 1988)

Langmuir isotherm (Ding and Alpay, 2000a)

$$q^*_{CO_2} = \frac{m_{CO_2}b_{CO_2}P_{CO_2}}{1+b_{CO_2}P_{CO_2}},\ \text{where } m_{CO_2} = 0.65\ \mathrm{mol/kg},\ b_{CO_2} = 2.36\times10^{-4}\exp\left[\frac{17{,}000}{R}\left(\frac{1}{T}-\frac{1}{673}\right)\right]\mathrm{Pa^{-1}}$$

(wet condition); $m_{CO_2} = 0.63\ \mathrm{mol/kg},\ b_{CO_2} = 1.69\times10^{-4}\exp\left[\frac{10{,}000}{R}\left(\frac{1}{T}-\frac{1}{673}\right)\right]\mathrm{Pa^{-1}}$ (dry condition)

Mass-transfer coefficient (Ding and Alpay, 2000a)

$$k_{CO_2} = \frac{15}{r_p^2}\frac{\epsilon_p D_p}{\epsilon_p + \rho_p RT(\partial q^*_{CO_2}/\partial P_{CO_2})},\ \text{in which } \rho_p = 1{,}300\ \mathrm{kg/m^3},\ D_p = 3.3\times10^{-7}\ \mathrm{m^2/s}$$

Bed effective conductivity k_z (Yagi et al., 1960; Malek and Farooq, 1997)

$$\frac{k_z}{k_g} = \frac{k_z^0}{k_g} + 0.75(Pr)(Re_p),\ \text{where}\ \frac{k_z^0}{k_g} = \epsilon_b + \frac{\epsilon_b}{0.139\epsilon_b - 0.0339 + 2/3(k_g/k_p)},\ Pr = \frac{C_{pg}\mu}{k_g},\ \text{and}$$

$$Re_p = \frac{\rho_g u\epsilon_b d_p}{\mu},\ \text{in which } k_p = 1\times10^{-2}\ \mathrm{J/cm\cdot s\cdot K} \text{ and } k_g = 2.5\times10^{-4}\ \mathrm{J/cm\cdot s\cdot K}$$

(Eucken formula, in Bird et al., 1960)

Wall-bed heat-transfer coefficient, U (Li and Finlayson, 1977)

$$\frac{2UR_0}{k_g} = 2.03Re_p^{0.8}\exp\left(-\frac{3d_p}{R_0}\right)\left(Re_p = 20-7{,}600,\ \frac{d_p}{2R_0} = 0.05-0.3\right),\ \text{and}$$

$$U = 6.15\frac{k_z^0}{2R_0} \text{ as } Re_p \to 0 \text{ (De Wasch and Froment, 1972)}$$

remaining CO_2 in the gas phase is adsorbed by the adsorbent.

During Steps 1 to 5, the feedgas temperature T_f and the wall temperature T_w are kept constant.

Theoretical Model

The theoretical model adopted for the sorption-enhanced reaction cyclic process is a nonisothermal, nonadiabatic, and nonisobaric operation, developed to describe both the steam–methane reforming (SMR) and the sorption-enhanced SMR (SE-SMR) processes. For the SE-SMR process, the reactions were assumed to take place on the surface of the catalyst. The model assumptions adopted are summarized below (Malek and Farooq, 1997; Silva and Rodrigues, 1998; Ding and Alpay, 2000b; Da Silva and Rodrigues, 2001):

1. The flow is represented by an axial-dispersed plug-flow model. Mass dispersion in the axial direction is considered, with negligible radial gradients. The axial dispersion coefficient was estimated from the correlation of Edwards and Richardson (1968), as shown in Table 2. Change of flow due to adsorption/desorption and reactions, as determined by the overall material balance, is taken into account. The gas is assumed to be an ideal gas.

2. Pressure distribution in the packed-bed adsorptive reactor was described by the mechanical energy equation.

3. The system is nonisothermal. The column wall and the feed stream are maintained at the same constant temperature. Thermal dispersion in the axial direction is considered, with negligible radial gradients. Axial thermal conductivity is estimated using the empirical correlation given by Yagi et al. (1960), as reproduced in Table 2. For a bed packed with spherical particles, the wall-bed heat-transfer coefficient, U, is given by De Wasch and Froment (1972) and Li and Finlayson (1977). The gas-phase and the catalyst/adsorbent particle are assumed to be in local thermal equilibrium at all times.

4. There exist five components (CH_4, H_2, CO_2, CO, and H_2O) in an inert carrier (N_2). The Langmuir model is adopted to describe the adsorption equilibrium for component CO_2. Hufton et al. (1999) and Ding and Alpay (2000a) reported that steam had a significant effect on the adsorption behavior of CO_2. In this article, two different sets of Langmuir adsorption parameters are used for wet and dry conditions (Ding and Alpay, 2000a), as shown in Table 2.

5. The linear deriving-force (LDF) model is used to represent the mass transport of CO_2 to the adsorbent. Table 2 also shows the correlation to evaluate the value of the LDF mass-transfer coefficient (Ding and Alpay, 2000a).

From the preceding assumptions, we can derive the following governing equations and the corresponding initial conditions and general boundary conditions for the five steps.

Based on Eq. 2a, the actual rates of r_i, $(r_i)_{\text{obv}}$, ($i = CH_4$, H_2O, H_2, CO_2, CO) can be expressed as

$$(r_i)_{\text{obv}} = \sum_{j=I}^{III} \upsilon_{ij}\eta_j R_j \quad (i = \text{CH}_4, \text{H}_2\text{O}, \text{H}_2, \text{CO}_2, \text{CO}), \quad (3)$$

where η_j is the effectiveness factor for reaction j (j = I, II, III).

Thus, the overall mass balance equation is

$$\epsilon_t \frac{\partial C}{\partial t} + \frac{\partial (uC)}{\partial z} + \rho_{\text{ad}} \frac{\partial \bar{q}_{\text{CO}_2}}{\partial t} - \rho_{\text{cat}} \sum_{i=1}^{5} \sum_{j=I}^{III} \upsilon_{ij}\eta_j R_j = 0 \quad (i = \text{CH}_4, \text{H}_2\text{O}, \text{H}_2, \text{CO}_2, \text{CO}), \quad (4)$$

where C is the total molar concentration in the bulk phase, ϵ_t is the total porosity of the packed bed, u is the superficial velocity, $\bar{q}_{\text{CO}_2}$ is the solid-phase concentration for CO_2 (average over an adsorbent particle), ρ_{ad} is the mass of adsorbent per bed volume, and ρ_{cat} is the mass of catalyst per bed volume. These densities of ρ_{ad} and ρ_{cat} are related to the bulk packing density ρ_b by $\rho_{\text{ad}} = \alpha\rho_b/(1+\alpha)$, $\rho_{\text{cat}} = \rho_b/(1+\alpha)$, where α is the mass ratio of the adsorbent and catalyst in the packed bed.

The kinetic-energy change is neglected in the mechanical-energy balance; then we have (Sereno and Rodrigues, 1993)

$$\frac{\partial}{\partial t}(\rho_g u) = -\frac{\partial P}{\partial z} - K_D u - K_V u|u|, \quad (5)$$

where ρ_g is the gas-phase density, and K_D and K_V are parameters corresponding to the viscous and kinetic pressure loss terms (see Table 2).

For component i ($\bar{q}_i = 0$, unless for $i = CO_2$), the mass balance for the packed-bed adsorptive reactor can be written as

$$\epsilon_t \frac{\partial C_i}{\partial t} + \frac{\partial (uC_i)}{\partial z} + \rho_{\text{ad}} \frac{\partial \bar{q}_i}{\partial t} - \rho_{\text{cat}} \sum_{j=I}^{III} \upsilon_{ij}\eta_j R_j = \epsilon_b \frac{\partial}{\partial z}\left(D_L C \frac{\partial y_i}{\partial z}\right) \quad (i = \text{CH}_4, \text{H}_2\text{O}, \text{H}_2, \text{CO}_2, \text{CO}), \quad (6)$$

where C_i is the molar concentration of gas-phase component i ($C_i = y_i C$), ϵ_b is the voidage of the bed, and D_L is the axial dispersion coefficient.

The LDF model is adopted to describe the mass-transfer rate of CO_2 to the adsorbent

$$\frac{\partial \bar{q}_{\text{CO}_2}}{\partial t} = k_{\text{CO}_2}(q^*_{\text{CO}_2} - \bar{q}_{\text{CO}_2}), \quad (7)$$

where k_{CO_2} is the LDF mass-transfer coefficient, and $q^*_{\text{CO}_2}$ is the equilibrium solid-phase concentration, which are respectively evaluated by the correlation given by Ding and Alpay (2000a) and the Langmuir isotherm (see Table 2).

The energy balance for the bed-volume element, including the heat-transfer to the column wall, is described as (Kikkinides et al., 1993; Ding and Alpay, 2000b)

$$\left[\epsilon_t C C_{vg} + (\rho_{\text{ad}} + \rho_{\text{cat}}) C_{ps}\right] \frac{\partial T}{\partial t} + C C_{pg} u \frac{\partial T}{\partial z} - \rho_{\text{ad}} \sum_{i=1}^{n} \left(-\Delta H_{\text{adi}} \frac{\partial \bar{q}_i}{\partial t}\right) - \frac{2U}{R_0}(T_w - T) - \rho_{\text{cat}} \sum_{i=1}^{5} \sum_{j=I}^{III} \upsilon_{ij}\eta_j R_j \Delta H_{Rj} = \frac{\partial}{\partial z}\left(k_z \frac{\partial T}{\partial z}\right), \quad (8)$$

where C_{pg} and C_{ps} are the gas- and solid-phase heat capacity, respectively, C_{vg} is the heat capacity of the gas phase at constant volume, k_z is the effective thermal conductivity, $-\Delta H_{\text{adi}}$ is the adsorption heat for component i (that is, CO_2), ΔH_{Rj} is the reaction heat of reaction j, U is the overall bed-wall heat-transfer coefficient, and R_0 is the inner radius of the reactor.

Initial conditions

At $t = 0,\ T = T_f,\ u = 0,\ q_i = 0,\ y_{H_2} = 1,\ y_i = 0,\ P_{H_2} = P_H,\ P_i = 0$ (i = CO, CO_2, H_2O, CH_4, N_2).

The final distributions of concentrations, temperature, pressure along the adsorptive reactor column for one step are the initial conditions for the next step.

General boundary conditions for the five steps

$$\left(\frac{\partial y_i}{\partial z}\right)_{z=0} = \delta_1, \qquad \left(\frac{\partial y_i}{\partial z}\right)_{z=L} = \delta_2 \tag{9a}$$

$$\left.\begin{array}{ll} (u)_{z=0} & \text{(for Steps 1,5)} \\ \left(\dfrac{\partial u}{\partial z}\right)_{z=0} & \text{(for Steps 2–4)} \end{array}\right\} = \delta_3,$$

$$\left.\begin{array}{ll} \left(\dfrac{\partial u}{\partial z}\right)_{z=L} & \text{(for Steps 1,5)} \\ (u)_{z=L} & \text{(for Steps 2–4)} \end{array}\right\} = \delta_4 \tag{9b}$$

$$\left.\begin{array}{ll} (P)_{z=0} & \text{(for Steps 1,2)} \\ \left(\dfrac{\partial P}{\partial z}\right)_{z=0} & \text{(for Steps 3–5)} \end{array}\right\} = \delta_5,$$

$$\left.\begin{array}{ll} \left(\dfrac{\partial P}{\partial z}\right)_{z=L} & \text{(for Steps 1,2)} \\ (P)_{z=L} & \text{(for Steps 3–5)} \end{array}\right\} = \delta_6 \tag{9c}$$

$$\left(\frac{\partial T}{\partial z}\right)_{z=0} = \delta_7, \qquad \left(\frac{\partial T}{\partial z}\right)_{z=L} = \delta_8, \tag{9d}$$

in which the expressions of δ for the five steps are listed in Table 3.

Simplification of Governing Equations

Assuming ideal-gas law $C = P/RT$, the following equation can be derived from Eq. 6

$$\frac{\partial y_i}{\partial t} = \frac{\epsilon_b}{\epsilon_t}\frac{D_L}{L^2}\left(\frac{\partial^2 y_i}{\partial \zeta^2} + \frac{1}{P}\frac{\partial P}{\partial \zeta}\frac{\partial y_i}{\partial \zeta} - \frac{1}{T}\frac{\partial T}{\partial \zeta}\frac{\partial y_i}{\partial \zeta}\right) - \frac{1}{\epsilon_t L}\left(u\frac{\partial y_i}{\partial \zeta} + y_i\frac{\partial u}{\partial \zeta} + \frac{uy_i}{P}\frac{\partial P}{\partial \zeta} - \frac{uy_i}{T}\frac{\partial T}{\partial \zeta}\right) - \frac{\rho_{\text{ad}}RT}{\epsilon_t P}\frac{\partial \bar{q}_i}{\partial t} + \frac{\rho_{\text{cat}}RT}{\epsilon_t P}\sum_{j=I}^{III}\upsilon_{ij}\eta_j R_j - \frac{y_i}{P}\frac{\partial P}{\partial t} + \frac{y_i}{T}\frac{\partial T}{\partial t}, \tag{10a}$$

where $\zeta = z/L$. The term $\partial \bar{q}_i/\partial t$ equals zero except for $i = CO_2$; $\partial \bar{q}_{CO_2}/\partial t$ is calculated by Eq. 7.

The flow velocity is derived from the overall material balance (Eq. 4)

$$\frac{\partial u}{\partial \zeta} = \frac{u}{T}\frac{\partial T}{\partial \zeta} - \frac{u}{P}\frac{\partial P}{\partial \zeta} - \frac{\rho_{\text{ad}}RTL}{P}\frac{\partial \bar{q}_{CO_2}}{\partial t} + \frac{2\rho_{\text{cat}}RTL}{P}(\eta_I R_I + \eta_{II} R_{II}) - \frac{\epsilon_t L}{P}\frac{\partial P}{\partial t} + \frac{\epsilon_t L}{T}\frac{\partial T}{\partial t}. \tag{10b}$$

The interbed pressure dynamics for the variable pressure steps are estimated using a linear dynamic pressure (Sereno and Rodrigues, 1993; Malek and Farooq, 1997)

$$\frac{\partial P}{\partial t} = \begin{cases} 0 & \text{(for step 1)} \\ -(P_H - P_L)/t_2 & \text{(for step 2)} \\ 0 & \text{(for step 3)} \\ 0 & \text{(for step 4)} \\ (P_H - P_L)/t_5 & \text{(for step 5).} \end{cases} \tag{10c}$$

Table 3. Values of δ for the Five Steps of the PSAR Cycle

Step	δ_1	δ_2	δ_3	δ_4	δ_5	δ_6	δ_7	δ_8
1. (Reaction + adsorption)	$-\dfrac{u_{10}(y_{fi} - y_i)}{\epsilon_b D_L}$	0	u_{10}	0	P_H	0	$-\dfrac{u_{10}CC_{pg}(T_f - T)}{k_z}$	0
2. (Reaction + desorption)	0	0	0	0	$P(t)$*	0	0	0
3. Desorption	0	$\dfrac{u_{30}(y_{fi} - y_i)}{\epsilon_b D_L}$	0	$-u_{30}$	0	P_L	0	$\dfrac{u_{30}CC_{pg}(T_f - T)}{k_z}$
4. Desorption	0	$\dfrac{u_{40}(y_{fi} - y_i)}{\epsilon_b D_L}$	0	$-u_{40}$	0	P_L	0	$\dfrac{u_{40}CC_{pg}(T_f - T)}{k_z}$
5.	0	$\dfrac{u_{50}(y_{fi} - y_i)}{\epsilon_b D_L}$	0	0	0	$P(t)$*	0	$\dfrac{u_{50}CC_{pg}(T_f - T)}{k_z}$

Note: All velocities u_{k0} ($k = 1, 2, \ldots, 5$) are taken as positive numbers, whatever the flow direction. The index k stands for the step number and the index 0 stands for the feed side in Steps 1, 3, 4, and 5 and outlet for Step 2.
*Equation 10c was used (linear ramp).

The mechanical energy balance (Eq. 5) is changed as (Ergun equation)

$$\frac{\partial P}{\partial \zeta} = L\left(-K_D u - K_V u|u|\right). \tag{10d}$$

Based on Eq. 8, the energy balance for the bed-volume element that includes the heat-transfer to the column wall is described as

$$\frac{\partial T}{\partial t} = \frac{1}{\left[\dfrac{\epsilon_t C_{vg} P}{RT} + (\rho_{\text{ad}} + \rho_{\text{cat}}) C_{ps}\right]} \times \left[\begin{array}{l} \dfrac{k_z}{L^2}\dfrac{\partial^2 T}{\partial \zeta^2} - \dfrac{C_{pg} P u}{RTL}\dfrac{\partial T}{\partial \zeta} + \rho_{\text{ad}}\left(-\Delta H_{\text{ad CO}_2}\right)\dfrac{\partial \bar{q}_{\text{CO}_2}}{\partial t} \\ +2\rho_{\text{cat}}(\eta_I R_I \Delta H_{RI} + \eta_{II} R_{II} \Delta H_{RII}) + \dfrac{2U}{R_0}(T_w - T) \end{array}\right]. \tag{10e}$$

Although the preceding model is a simplification of the real situation, it allows us to investigate the whole cyclic process for fine catalyst/adsorbent particles packed in the adsorptive reactor with small diameter.

Numerical Method

The model equations were numerically solved by the orthogonal collocation method for the continuous hydrogen production in the PSA reactor. Because of the presence of steep composition gradients within the bed and the periodic reversal in the direction of the gas flow, in this simulation 31 axial collocation points for the packed-bed adsorptive reactor were selected in order to obtain a stable numerical solution.

At all collocation points, Eqs. 10b and 10d are discretized into a set of linear algebraic equations that are solved numerically by the Gauss method in order to obtain the velocity and pressure distributions along the adsorptive reactor. Equations 10a and 10e are discretized in the axial direction, leading to a set of ordinary differential equations that are integrated in the time domain using Gear's stiff variable step integration routine in order to obtain the effluent mole fraction and temperature histories and the concentration and temperature profiles along the adsorptive reactor.

The sequence for solving numerically the PSA reactor at each step is as follows:

1. Calculate the reaction rates using Eqs. 1a, 1b, 1c
2. Calculate the pressure derivative using the linear dynamic model Eq. 10c
3. Calculate the adsorptive loading derivative by Eq. 7
4. Solve Eq. 10b for the velocity
5. Solve Eq. 10d for the pressure
6. Solve Eqs. 9a and 9d for the boundary conditions
7. Solve Eq. 10a for the species mole fraction derivative
8. Solve Eq. 10e for the temperature derivative.

At the end of each step, the gas- and solid-phase component concentrations, temperature, and pressure were stored

Table 4. Reference Parameters Values Used in the Simulations for Step 1

Parameters (Constants)	Values	
b_{CO_2}*	2.36×10^{-4} Pa^{-1} (wet condition) 1.69×10^{-4} Pa^{-1} (dry condition)	Change with T
C_{pg}*	42 J/mol·K	Constant
C_{ps}*	850 J/kg·K	Constant
d_p*	5×10^{-4} m	Constant
D_L**	1.6×10^{-5} m^2/s	Change with u
R_0*	0.0125 m	Constant
K_D**	42,103 N·s/m^4	Constant
K_V**	21,966 N·s^2/m^5	Change with T, P
k_z*	0.29 J/m·s·K	Change with u
$\Delta H_{\text{ad}\text{CO}_2}$*	−17,000 J/mol	Constant
m_{CO_2}*	0.65 mol/kg (wet condition) 0.63 mol/kg (dry condition)	Constant
P_H*	445.7 kPa	Constant
P_L†	125.7 kPa	Constant
T_f*	723 K	Constant
T_w†	723 K	Constant
U**	71 J/m^2·K	Change with u
ϵ_b*	0.48	Constant
ϵ_p* (for adsorbent)	0.24	Constant
ϵ_t*	0.64	Constant
μ*	2.87×10^{-5} Pa·s	Constant
ρ_{ad}†	498 kg/m^3	Constant
ρ_{cat}†	249 kg/m^3	Constant
η_j*	1.0	Constant

*Data from Ding and Alpay (2000a,b).
**Data evaluated from Table 2.
†Present work.

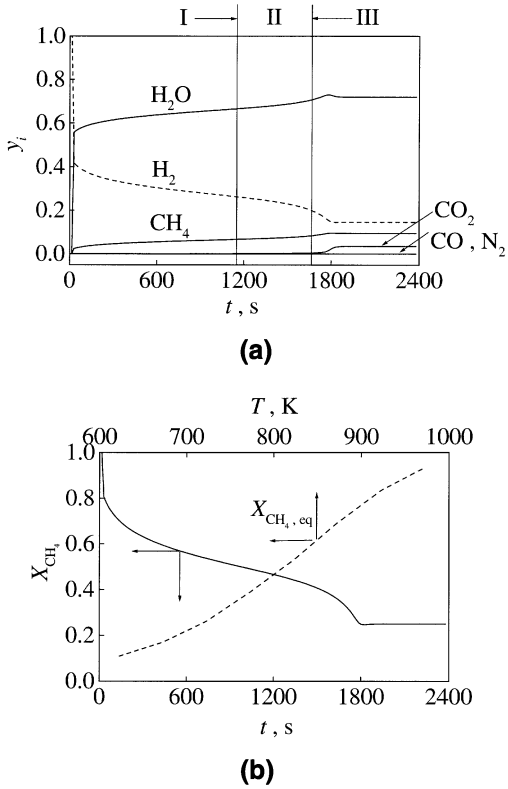

Figure 2. (a) Typical effluent mole fraction y_i and (b) methane conversion X_{CH_4} vs. time t for Step 1.

$P_H = 445.7$ kPa; $T_f = T_w = 450$°C; $L = 2$ m; $u_{10} = 0.05$ m/s; $H_2O/CH_4 = 6$; $\rho_{ad} = 498$ kg/m^3; $\rho_{cat} = 249$ kg/m^3; $m_{CO_2} = 0.65$ mol/kg; $b_{CO_2} = 2.36\times10^{-4}$ Pa^{-1}.

and used as the initial conditions for the next step in one cycle.

The adsorption behavior of CO_2 onto the adsorbent under wet and dry conditions is different (Hufton et al., 1999; Ding and Alpay, 2000a); therefore, we take the data under wet conditions for Steps 1 and 2, and the data under dry condition for Steps 3 to 5.

The criteria to switch from one step to the next are: the average purity of hydrogen product for Step 1 equals 80%, and the exit mole fraction of CO_2 for Step 3 must be lower than 1.0×10^{-2}. The time duration of Steps 2, 4, and 5 were all set in the 100s. The criterion for cyclic steady-state operation was based on the average purity of the hydrogen product.

Results and Discussion

Adsorption-enhanced steam–methane reforming process

Figure 2 shows typical effluent mole fraction, y_i (Figure 2a), and methane conversion (Figure 2b) as a function of time, t, for the adsorption-enhanced reaction process at $P_H = 445.7$ kPa, $L = 2$ m, $T_f = T_w = 450$°C, $u_{10} = 0.05$ m/s, $H_2O/CH_4 = 6$ (the mole fraction of inert gas is about 0.001), and the mass ratio of adsorbent to catalyst = 2; the other reference data are listed in Table 4.

The basic parameters for the simulation of the adsorption-enhanced reaction step are selected from Ding and Alpay (2000a,b). The diameters of the adsorbent and catalyst, d_p, are chosen as 0.5 mm. To calculate the effectiveness factors, we should consider the catalyst and its properties in more detail. For our simulation system, the catalyst is uniform and small in size; for convenience, we chose $\eta_j = 1.0$ and assumed that η_j is the same for different reactions. The properties of the gas mixture change with pressure, temperature, and other operating conditions; the reference values for Step 1 are listed in Table 4.

In Figure 2a, it is evident that the whole region can be divided into three zones according to the adsorption behavior of CO_2. (I) The adsorption-enhanced reaction zone, where the effluent mole fraction of CO_2 is lower (mole fraction is about 9.4×10^{-3}), adsorption enhances the conversion of methane, and the effluent mole fraction of hydrogen at the exit is higher; at the same time, the coproduction of CO is suppressed (Hufton et al., 1999). (II) The breakthrough zone of CO_2, where the mole fraction of CO_2 increases from 9.4×10^{-3} to 3.8×10^{-2}, the adsorbent is nearly saturated by CO_2 in the operation zone of the reactor, the enhancement is not evident, and the purity of hydrogen at the effluent gas drops rapidly. (III) The equilibrium state zone, where the adsorbent is saturated almost entirely by CO_2, the operation mode is the same as the conventional one, that is, the steam–methane reforming reaches the steady state. At the steady state, the conversion of methane reaches 24.5%, which is in reasonable agreement with the experimental data of Ding and Alpay (2000b) (24.0%) and Hufton et al. (1999) (28.0%). At the initial state of the adsorption-enhanced reaction zone (for $0 \sim 300$ s), methane conversion is larger than 65%, while for conventional reactor (without adsorbent), the reaction temperature should be controlled above 600°C in order to reach the same conversion (Figure 2b):

y_i (dry basis) and the conversion of methane X_{CH_4} are respectively defined as

$$y_i\ (\text{dry basis}) = \frac{y_i}{1 - y_{H_2O}} \tag{11a}$$

$$X_{CH_4} = \frac{\text{Feed of } CH_4\ (\text{mol/s}) - \text{effluent of } CH_4\ (\text{mol/s})}{\text{Feed of } CH_4\ (\text{mol/s})} = 1 - \left(\frac{RT_f}{u_{10}P_H y_{0CH_4}}\right)_{\text{feed}} \left(\frac{uPy_{CH_4}}{RT}\right)_{\text{outlet}}. \tag{11b}$$

At the equilibrium state (without adsorbent), we can derive the following relationship to check the simulation results

$$X_{eq,\,CH_4} = \frac{1 - y_{eq,\,CH_4}(\text{dry basis})}{1 + 4y_{eq,\,CH_4}(\text{dry basis})}, \tag{11c}$$

that is, at the equilibrium state, the result from Eq. 11b should be equal to that from Eq. 11c.

The adsorbent, which can adsorb CO_2 at high temperature, is usually made of K_2CO_3–hydrotalcite (Hufton et al., 1999). At 450°C, the saturated CO_2 adsorption capacity is

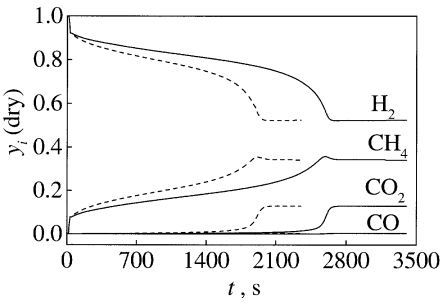

Figure 3. Effect of adsorbent capacity for CO_2 on H_2 purity of effluent gas vs. time for Step 1.

Common conditions: $P_H = 445.7$ kPa; $T_f = T_w = 450$°C; $L = 2$ m; $u_{10} = 0.05$ m/s; $H_2O/CH_4 = 6$; $\rho_{ad} = 498$ kg/m^3; $\rho_{cat} = 249$ kg/m^3. Solid line: $m_{CO_2} = 0.85$ mol/kg; $b_{CO_2} = 3.94 \times 10^{-4}$ Pa^{-1} (Hufton et al., 1999). Dashed line: $m_{CO_2} = 0.65$ mol/kg; $b_{CO_2} = 2.36 \times 10^{-4}$ Pa^{-1} (Ding and Alpay, 2000b).

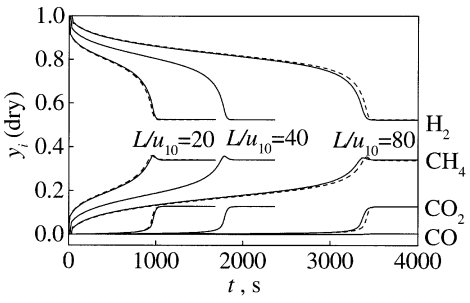

Figure 5. Effect of residence time on H_2 purity vs. time for Step 1.

Common conditions: $P_H = 445.7$ kPa; $T_f = T_w = 450$°C; $H_2O/CH_4 = 6$; $\rho_{ad} = 498$ kg/m^3; $\rho_{cat} = 249$ kg/m^3; $m_{CO_2} = 0.65$ mol/kg; $b_{CO_2} = 2.36 \times 10^{-4}$ Pa^{-1}. Solid line: $L = 2$ m with change of feed velocity u_{10}; dashed line: $u_{10} = 0.05$ m/s with change of length L.

about 0.5 ~ 1.0 mol/kg. Figure 3 shows the effect of the CO_2 adsorption capacity on the effluent concentrations from the adsorptive reactor, where the solid lines were calculated with $m_{CO_2} = 0.85$ mol/kg, $b_{CO_2} = 3.94 \times 10^{-4}$ Pa^{-1} (Hufton et al., 1999), and the dashed lines with $m_{CO_2} = 0.65$ mol/kg, $b_{CO_2} = 2.36 \times 10^{-4}$ Pa^{-1} (Ding and Alpay, 2000a). It is evident that the adsorbent with higher CO_2 adsorption capacity will lead to higher methane conversion and higher hydrogen purity in the product gas. However, it is difficult to improve the adsorption capacity of the adsorbent at high temperature; it is better to adjust the packing density of the adsorbent and the catalyst to enhance the methane conversion. In Figure 4, a comparison is made between the performance of the adsorptive reactor under two different packing densities, that is, between the data of Ding and Alpay (2000a) and that of Hufton et al. (1999). The isotherm parameters use the relevant ones, that is, those of Ding and Alpay (2000a) for simulations with a bulk packing density of 747 kg/m^3, and those of Hufton et al. (1999) when using a bulk packing density of 1,538 kg/m^3. Figure 4 shows that the performance improvement could be obtained by the use of a superior adsorbent

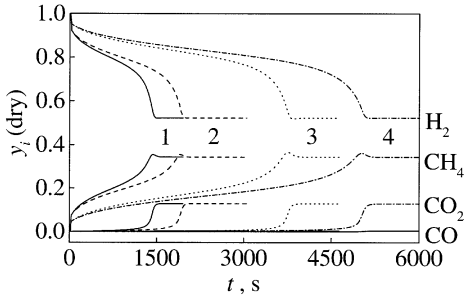

Figure 4. Effect of density of adsorbent and catalyst on H_2 purity of effluent gas vs. time t for Step 1.

Common conditions: $P_H = 445.7$ kPa; $T_f = T_w = 450$°C; $L = 2$ m; $u_{10} = 0.05$ m/s; $H_2O/CH_4 = 6$. Line 1 ($\rho_{ad}/\rho_{cat} = 1$; solid line) and line 2 ($\rho_{ad}/\rho_{cat} = 2$; dashed line): bulk packing density 747 kg/m^3, with $m_{CO_2} = 0.65$ mol/kg and $b_{CO_2} = 2.36 \times 10^{-4}$ Pa^{-1} (Ding and Alpay, 2000b). Line 3 ($\rho_{ad}/\rho_{cat} = 1$; dotted line) and line 4 ($\rho_{ad}/\rho_{cat} = 2$; dashed-dot line): bulk packing density 1,538 kg/m^3 with $m_{CO_2} = 0.85$ mol/kg and $b_{CO_2} = 3.94 \times 10^{-4}$ Pa^{-1} (Hufton et al., 1999).

[lines 3 and 4: bulk packing density 1,538 kg/m^3 with $m_{CO_2} = 0.85$ mol/kg, $b_{CO_2} = 3.94 \times 10^{-4}$ Pa^{-1} for Hufton et al. (1999); lines 1 and 2: bulk packing density 747 kg/m^3 with $m_{CO_2} = 0.65$ mol/kg, $b_{CO_2} = 2.36 \times 10^{-4}$ Pa^{-1} for Ding and Alpay (2000a)].

In addition, controlling the residence time (L/u_{10}) of the feedgas in the adsorptive reactor will also be a good method for improving the H_2 purity in the effluent gas and the productivity. Increasing the residence time of the feed gas passing through the adsorptive reactor by increasing the length, L, or by decreasing the feed velocity, u_{10}, leads to a higher purity of the H_2 product gas, and better productivity can be obtained during the adsorption-enhanced reaction process, as shown in Figure 5. The S/C (steam/methane) ratio is also a key parameter; a higher S/C ratio will be favorable for obtaining higher purity H_2, as shown in Figure 6.

For a given system (specified the adsorbent and the temperature), increasing the packing density, the adsorbent/catalyst ratio, and the residence time favors the production of high-purity H_2.

Hufton et al. (1999) carried out experiments for the production of hydrogen by the sorption-enhanced steam–methane reforming process, where a long reactor with higher packing adsorbent and catalyst densities was selected (see Table 5). Higher purity of H_2 is obtained due to small feed velocity and adsorbent with higher CO_2 adsorption capacity. When the net H_2 productivity is 0.8 mol/kg (solid), the purity of the H_2 product is 96%. The simulation results based on their experimental conditions are shown in Figure 7. If controlled, the reaction time is 995 s, the same net H_2 productivity (that is, 0.8 mol/kg of the solid) can be obtained, and the H_2 product purity is 92%.

Here, the average purity of hydrogen (dry basis), y_{H_2} (av), at the given operating time, t_1, is calculated by

$$y_{H_2}(av) = \frac{1}{\int_0^{t_1} \left(\frac{Pu\left(1 - y_{H_2O}\right)}{RT} \right)_{outlet} dt} \int_0^{t_1} \left(\frac{Puy_{H_2}}{RT} \right)_{outlet} dt. \tag{11d}$$

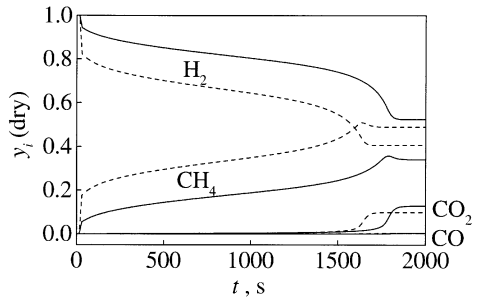

Figure 6. Effect of mole ratio of steam to methane on H_2 purity of effluent gas vs. time for Step 1.

Common conditions: $P_H = 445.7$ kPa; $T_f = T_w = 450$°C; $L = 2$ m; $u_{10} = 0.05$ m/s, $m_{CO_2} = 0.65$ mol/kg; $b_{CO_2} = 2.36 \times 10^{-4}$ Pa^{-1}. Solid line: $H_2O/CH_4 = 6$; dashed line: $H_2O/CH_4 = 3$.

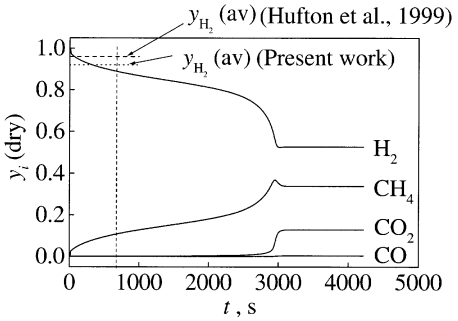

Figure 7. Effluent mole fraction y_i vs. time based on experimental data of Hufton et al. (1999) for Step 1.

$P_H = 445.7$ kPa; $T_f = T_w = 450$°C; $L = 1.067$ m; $u_{10} = 0.037$ m/s; $H_2O/CH_4 = 6$; $\rho_{ad} = 769$ kg/m^3; $\rho_{cat} = 769$ kg/m^3; $m_{CO_2} = 0.85$ mol/kg; $b_{CO_2} = 3.94 \times 10^{-4}$ Pa^{-1}.

Ding and Alpay (2000b) also carried out experiments. Figure 8 shows a comparison of our simulation results with their experimental data (for the experimental conditions, see Table 5). The prediction is good except in the initial period; the deviation from the experimental data in the initial period is partly due to the lack of the adsorption data of CO_2 at relatively low concentrations. For their experimental conditions, the H_2 purity in the effluent gas is lower due to the shorter residence time of feed gas in the adsorptive reactor.

Continuous production of H_2 under cyclic steady state

For industrialization, the high purity of H_2 product gas should be continuously produced from the adsorptive reactor under cyclic steady state; here a five-step one-bed cyclic process is adopted. In this cyclic process, the adsorption-enhanced steam-methane reforming is performed at high pressure ($P_H = 445.7$ kPa) and the regeneration of the adsorbent that was saturated with CO_2 is carried out at low pressure ($P_L = 125.7$ kPa), where the adsorptive reactor is purged first with methane, and then with part of the hydrogen product gas. In the simulation, the adsorptive reactor length is 2 m with a diameter of 25 mm, which is packed with the catalyst and adsorbent mixture (the densities of the catalyst and adsorbent are 249 kg/m^3 and 498 kg/m^3, respectively). The adsorption equilibrium uses data from Ding and Alpay (2000a). It is assumed that the linear change of the pressure occurs with time in the depressurization step and the pressurization step (Eq. 10c).

It should be noted that the adsorptive reactor is saturated with H_2 only at Step 1 of the first cycle.

Figure 9 shows the changes in pressure, temperature, and the flow velocity at $z = 0$ m, in the middle of the bed at $z = 1$ m, and at the other extremity of the bed ($z = 2$ m) during one cycle. We take the 15th cycle, which is at the cyclic steady state for the continuous production of hydrogen, as an example. The negative velocity means that the flow is in the countercurrent direction to that of the feed gas flow. For Step 1, the feed velocity is $u_{10} = 0.05$ m/s, the operation time is controlled at $t_1 = 1{,}000$ s in order to obtain greater than 80% average purity of hydrogen in the effluent gas mixture (impure H_2 50–90% is acceptable with fuel cell applications as long as the CO level is kept below 30 ppm) (Hufton et al., 2000). The countercurrent depressurization time is set to be $t_2 = 100$ s, the countercurrent purge time with methane is controlled at $t_3 = 900$ s based on the exit mole fraction of CO_2, and the countercurrent purge time (t_4) with part of the

Table 5. Experimental Conditions from the Literature

	Ding and Alpay (2000a,b)	Hufton et al. (1999)
Mole ratio H_2O/CH_4	6	6
Reactor length L (m)	0.22	1.067
ID of reactor $2R_0$ (mm)	12.7	38
Dia. of particles d_p (mm)	0.5	3
Effectiveness factor η_j	1.0	0.8*
Superficial velocity u_{10} (m/s)	0.13	0.037
Dens. of adsorbent ρ_{ad} (kg/m^3) in ads. reactor	609	769
Dens. of catalyst ρ_{cat} (kg/m^3) in ads. reactor	139	769
Parameter for adsorption equil. m_{CO_2} (mol/kg)	0.65	0.85
Parameter for adsorption equil. b_{CO_2} (Pa^{-1})	2.36×10^{-4}	3.94×10^{-4}

*Xiu et al. (2002).

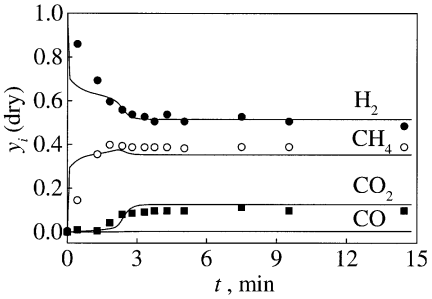

Figure 8. Comparison of simulated results with experimental data of Ding and Alpay (2000b) for Step 1.

$P_H = 445.7$ kPa; $T_f = 450$°C; $T_w = 457$°C; $L = 0.22$ m; $u_{10} = 0.13$ m/s; $H_2O/CH_4 = 6$; $\rho_{ad} = 609$ kg/m^3; $\rho_{cat} = 139$ kg/m^3; $m_{CO_2} = 0.65$ mol/kg; $b_{CO_2} = 2.36 \times 10^{-4}$ Pa^{-1}. Solid line: simulated results; points: experimental data (Ding and Alpay, 2000b).

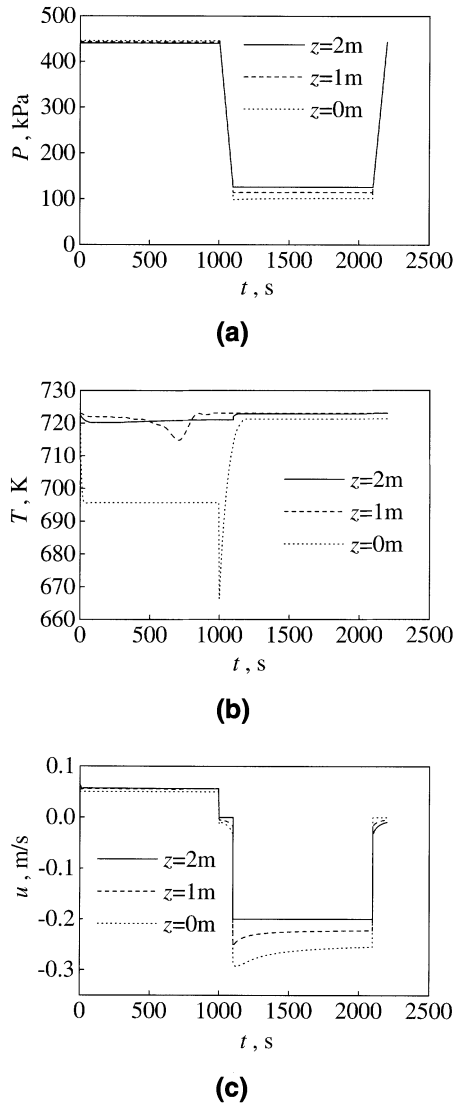

Figure 9. (a) Pressure, (b) temperature, and (c) velocity histories in the adsorptive reactor for the 15th cycle at various axial positions.

Adsorptive reactor conditions: $P_H = 445.7$ kPa; $T_f = T_w = 450$°C; $L = 2$ m; $\rho_{cat} = 249$ kg/m^3; $\rho_{ad} = 498$ kg/m^3 with $m_{CO_2} = 0.65$ mol/kg; $b_{CO_2} = 2.36 \times 10^{-4}$ Pa^{-1}. Cyclic operation conditions: $P_H = 445.7$ kPa; $P_L = 125.7$ kPa; $T_f = T_w = 450$°C; $u_{10} = 0.05$ m/s; $u_{30} = u_{40} = 0.2$ m/s; $t_1 = 1{,}000$ s; $t_3 = 900$ s; $t_2 = t_4 = t_5 = 100$ s; $H_2O/CH_4 = 6$.

hydrogen product gas and the countercurrent pressurization time (t_5) are set to be 100 s, respectively.

As shown in Figure 9a, for the high-pressure adsorption/reaction step (Step 1) and the low-pressure purge steps (Steps 3 and 4), the pressure drop along the adsorptive reactor is higher for a higher gas velocity. It is 5.7 kPa with 0.05 m/s feed gas velocity for Step 1 and 24.8 kPa with 0.2 m/s purge gas velocity for Steps 3 and 4.

The temperature change, which is caused by the endothermic reaction and adsorption, will be noticed in the high pressure adsorption/reaction step (Step 1) and the depressurization step (Step 2), as shown in Figure 9b. However, in the purge step (Step 3), the temperature change along the adsorptive reactor is observed only at the initial purge stage (about 200 s) due to the lower rate of CO_2 desorption from the adsorbent.

The number of moles increases for the steam–methane reforming reaction, therefore the output velocity from the reactor ($z = 2$ m) is higher than the feed velocity ($z = 0$ m) in the high-pressure adsorption/reaction step (Step 1), as shown in Figure 9c. At the initial purge stage, the change in output velocity ($z = 0$ m) is significant due to the desorption of CO_2 from the adsorbent, then the change is slow, and the output velocity is higher than the input velocity ($z = 2$ m). In the depressurization step, the output velocity ($z = 0$ m) increases with time, while in the pressurization step, the input velocity ($z = 2$ m) decreases with time.

Figure 10 shows the temperature, pressure, and velocity distributions along the adsorptive reactor at the end of the high pressure adsorption/reaction step (Step 1; Figure 10a), the countercurrent blowdown step (Step 2; Figure 10b), the purge step (Steps 3 and 4; Figure 10c), and the repressurization step (Step 5; Figure 10d).

Figure 11a shows the effluent mole fractions, y_i (dry), for the first cycle (solid lines), the 2nd, 5th, and 15th cycles (dotted lines) from the adsorptive reactor in Step 1 during the continuous production of H_2 under the operating conditions just mentioned. The purity of H_2 in the product gas (dry basis) in the first cycle is higher than that in the next cycles since the first cycle uses the fresh adsorbent. After regeneration, the adsorption capacity of the adsorbent will decrease slightly due to the remaining CO_2 in the adsorbent; therefore, the purity of the hydrogen will decrease. Figure 11b shows the average purity of the H_2 in the product gas obtained from Step 1 during the continuous production process as a function of the cycle number n. The average purity of the H_2 in the product gas (dry basis), y_{H_2} (av), will decrease with the cycle number. However, the cyclic steady state is reached quickly in our simulation conditions, as shown in Figure 11b; 15 cycles are sufficient to reach the cyclic steady state for the following criterion when $n \geq 15$:

$$\left| \frac{y_{H_2}^{(n)}(av) - y_{H_2}^{(n-1)}(av)}{y_{H_2}^{(n)}(av)} \right| \leq 1.0 \times 10^{-4}, \qquad (12)$$

where n is the number of the cycle.

At the cyclic steady state, hydrogen gas with an average purity of over 80%, with traces of the CO and CO_2, can be continuously produced; the productivity of hydrogen is about 0.63 mol/kg (solid) in one cycle.

Here, the productivity of H_2 per gram of solid in one cycle is calculated by

$$\text{mol } H_2/\text{g (solid)} = \frac{\int_0^{t_1} \left(\frac{Puy_{H_2}}{RT} \right)_{\substack{\text{Outlet} \\ \text{step 1}}} Adt - \left(\frac{P_H u_{40} y_{H_2} A t_4}{RT} \right)_{\substack{\text{Input} \\ \text{step 4}}} - \int_0^{t_5} \left(\frac{Pu_{50} y_{H_2}}{RT} \right)_{\substack{\text{Input} \\ \text{step 5}}} Adt}{AL(\rho_{ad} + \rho_{cat})} = 0.63 \text{ mol/kg (solid)}. \qquad (13)$$

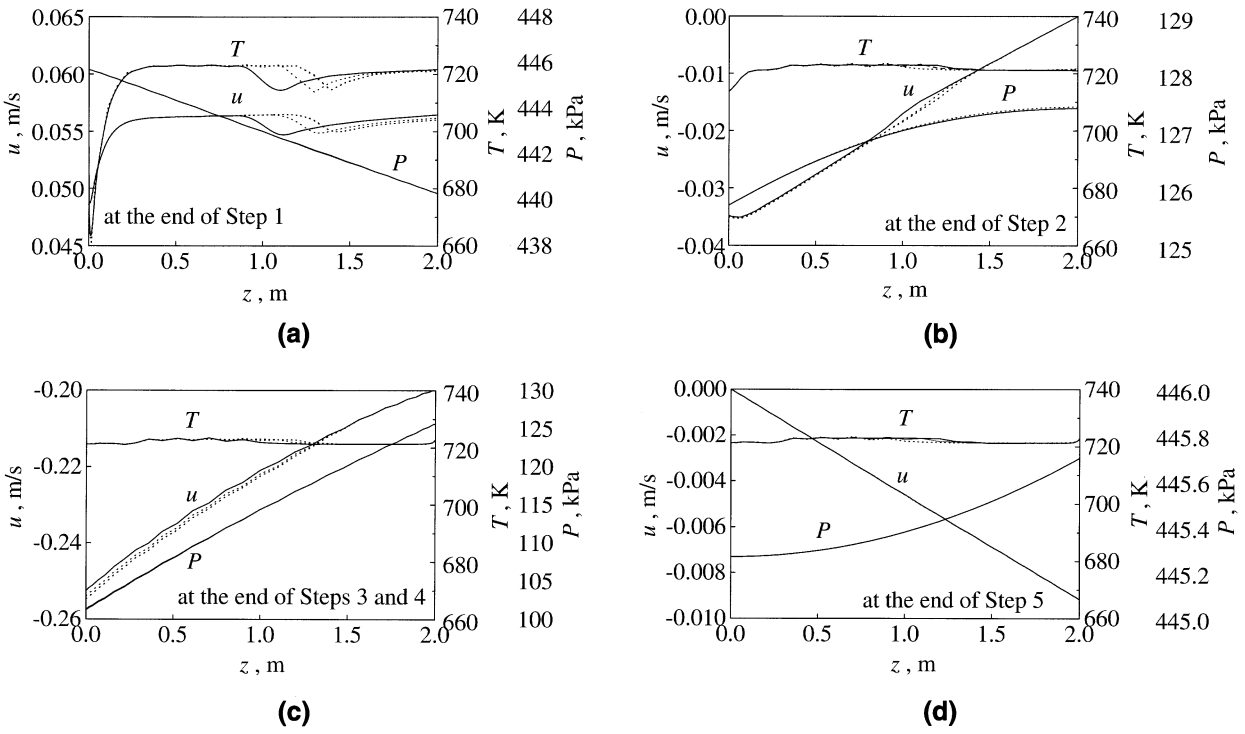

Figure 10. Pressure, temperature, and velocity axial distributions in cyclic process.

(a) At the end of Step 1; (b) at the end of Step 2; (c) at the end of Steps 3 and 4; (d) at the end of Step 5. The adsorptive reactor conditions and the cyclic operation conditions are the same as in Figure 9. Solid line: 1st cycle; dotted line: 2nd, 5th, 15th cycles.

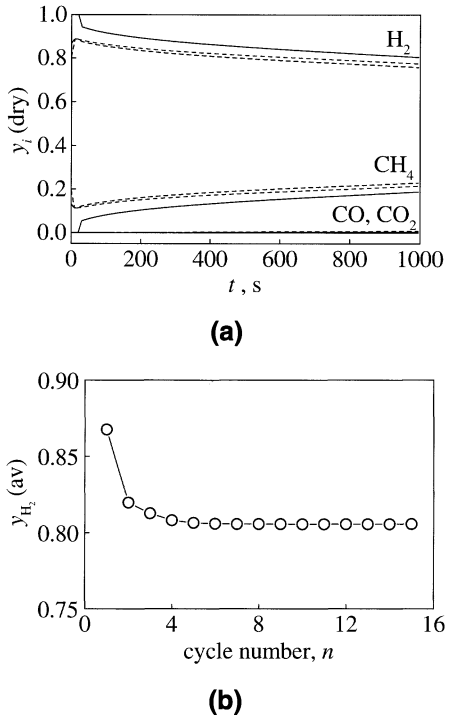

Figure 11. (a) Effluent mole fraction y_i vs. time t in Step 1 for the 1st, 2nd, 5th, and 15th cycles; (b) and average purity of H_2 in product gas vs. cycle number n.

The adsorptive reactor conditions and the cyclic operation conditions are the same as in Figure 9. (a) Solid line: 1st cycle; dotted line: 2nd, 5th, 15th cycles.

The regeneration of the adsorbent that is saturated with CO_2 in Step 1 should be a key step for the continuous production of high-purity hydrogen. If the regeneration is not enough, it is impossible to continuously produce high-purity hydrogen in the next cycle. We purge the adsorptive reactor with methane at a lower pressure to desorb CO_2 from the adsorbent (Step 3), and only a small fraction of hydrogen product gas is used to remove the remaining methane from the interparticle space of the reactor near the end of the purge step (Step 4). Figure 12 shows the CO_2 effluent mole fraction vs. time during the two purge steps. It is obvious that only in the initial period of the purge ($0 \sim 400$ s) is the CO_2 desorption rate faster; after 600 s the desorption rate is slow, which means a longer purge time is needed.

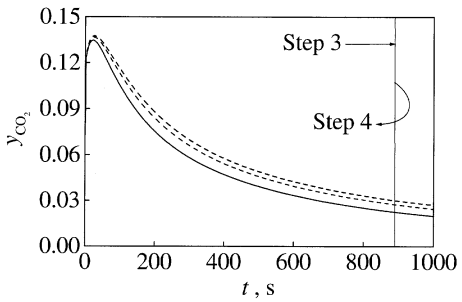

Figure 12. Effluent CO_2 mole fraction vs. time in Steps 3 and 4 in cyclic process.

The adsorptive reactor conditions and the cyclic operation conditions are the same as in Figure 9. Solid line: 1st cycle; dotted line: 2nd, 5th, and 15th cycles.

Carvill et al. (1996) pointed out that at least two parallel reactors are needed to run the cycle in a continuous mode. The cycle times for the steps are designed so that one reactor undergoes Step 1 for a period of time while the companion reactor undergoes Steps 2–5 during the same period of time. Our simulation results could not meet this condition, since $t_1 = 1{,}000$ s and $\sum_{i=2}^{5} t_i = 1{,}200$ s. The reason is that regeneration of the adsorbent is difficult; increasing the velocity of the carrying gas will favor the regeneration process, but lead to a higher pressure drop along the adsorptive reactor. Therefore, it is necessary to find a high-efficiency regeneration method. It should be noted that our process could be operated continuously by using two beds: when one bed is in Steps 5 and 1 ($t_1 + t_5 = 1{,}100$ s), the other is in Steps 2, 3, and 4 ($t_2 + t_3 + t_4 = 1{,}100$ s).

Figures 13a and 13b show CO_2 mole fraction distributions in the gas- and solid-phases along the adsorptive reactor at the end of each step. After the high-pressure adsorption/reaction step (Step 1), the adsorption front for CO_2 is located at about $z = 1.1$ m, as shown in Figure 13b, that is, the adsorbent between $z = 0$ and 1.1 m is saturated with CO_2, so the length of the unused bed (LUB) of the packed bed is $(2 - 1.1)/2 = 0.45$. During the countercurrent depressurization step (Step 2), the reversible reactions and CO_2 desorption take place simultaneously, the mole fraction of CO_2 in the gas-phase increases rapidly (Figure 13a), but the concentration of CO_2 in the solid-phase decreases slightly, and the distribution of CO_2 spreads (Figure 13b). In the purge step, the first purge is with methane (Step 3), and the second purge with a part of the hydrogen product gas (Step 4) to replace the remaining methane in the interparticle space of the adsorptive reactor. With two purge steps, the CO_2 in the adsorbent is desorbed and taken away by the inert gas; the adsorbent is regenerated and the CO_2 concentration in the adsorbent drops to an acceptable level, as shown in Figures 13a and 13b.

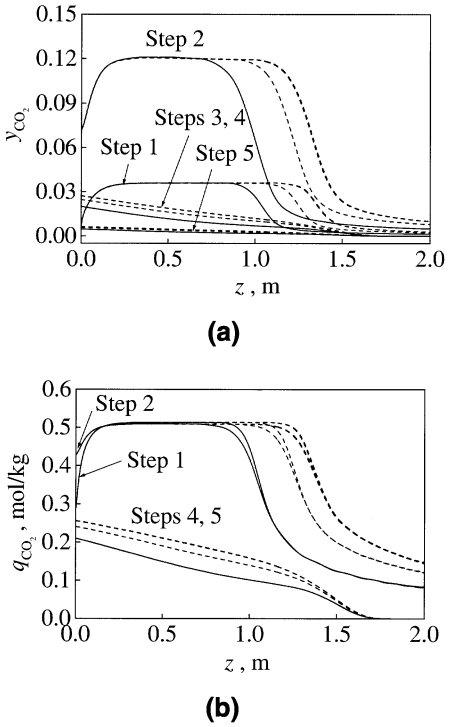

Figure 13. (a) Mole fraction of CO_2 in the gas phase vs. z, and (b) CO_2 adsorbent concentration vs. axial distance of reactor at the end of each step in the cyclic process.

The adsorptive reactor conditions and the cyclic operation conditions are the same as in Figure 9. Solid line: 1st cycle; dashed line: 2nd, 5th, 15th cycles.

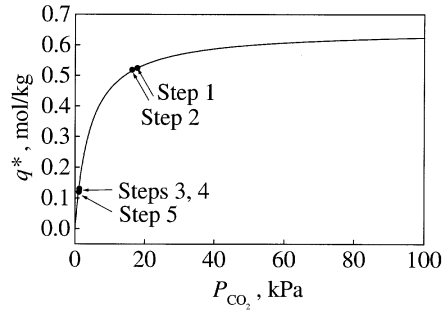

Figure 14. Operating points of partial pressure of CO_2 at the end of steps for one cycle: the adsorptive reactor conditions and the cyclic operation conditions are the same as in Figure 9.

In the last step of one cycle, that is, the pressurization step (Step 5), the adsorptive reactor is pressurized with part of the hydrogen product gas to a high pressure, P_H. Increasing pressure always favors the adsorption of CO_2; therefore, the CO_2 concentration in the gas-phase will decrease after the pressurization step, as shown in Figure 13a, but the CO_2 concentration in the adsorbent decreases only slightly (Figure 13b). After the pressurization step, the next cycle will start.

Figure 14 shows that Step 2 (countercurrent depressurization from $P_H = 445.7$ kPa to $P_L = 125.7$ kPa, operating time $t_2 = 100$ s) makes a minor contribution to the desorption of CO_2, because the partial pressures of CO_2 (about 17.8 kPa at the end of Step 1, $y_{CO_2} \approx 0.04$, and 16.3 kPa at the end of Step 2, $y_{CO_2} \approx 0.13$) are in the saturated region of the CO_2 isotherm. After Steps 3 and 4 (operating pressure $P_L = 125.7$ kPa, operating time $t_3 + t_4 = 1{,}000$ s, first purge with methane for $t_3 = 900$ s, purge velocity $u_{30} = 0.2$ m/s, then purge with hydrogen for $t_4 = 100$ s, purge velocity $u_{40} = 0.2$ m/s), the mole fraction of CO_2 in the gas-phase and the CO_2 concentration in the solid-phase decrease significantly, as shown in Figures 13a and 13b. This is because the fresh methane and hydrogen can reduce the partial pressure of CO_2 in the bulk phase (the partial pressures of CO_2 are 1.26 kPa at the end of Step 4 and 1.14 kPa at the end of Step 5, and the corresponding equilibrium solid concentrations are 0.13 mol/kg and 0.12 mol/kg, respectively).

Methane is lost in the first three steps. To measure the methane efficiency, we calculate the unused CH_4 in one cycle as follows

$$\text{Unused } CH_4 \text{ in one cycle} = \frac{\text{Feed of } CH_4 \text{ in Steps 1 and 3} - \text{Consumption of } CH_4 \text{ in Step 1}}{\text{Feed of } CH_4 \text{ in Steps 1 and 3}} = 0.92. \quad (14)$$

That is to say that 0.92 methane is lost compared to the methane fed. But the methane loss does not impact the viability of this system, because (1) the effluent gas from Steps 2 and 3, containing unrecovered H_2 and the mixture of CH_4, H_2O, CO, and CO_2 can be used as part of the fuel required to supply the heat of the endothermic SMR reaction, and (2) CH_4 can be replaced by steam or other inert gas in Step 3 (Hufton et al., 1999). If CH_4 is replaced by steam in Step 3, the unused CH_4 in one cycle is

$$\text{Unused } CH_4 \text{ in one cycle} = \frac{\text{Feed of } CH_4 \text{ in Step 1} - \text{Consumption of } CH_4 \text{ in Step 1}}{\text{Feed of } CH_4 \text{ in Step 1}} = 0.36. \quad (14a)$$

In conclusion, under cyclic steady-state operation conditions, H_2 product gas of 80% average purity can be continuously produced from a 2-m-long adsorptive reactor. Increasing the length of the adsorptive reactor produces higher purity H_2 product gas, but the regeneration of the adsorbent is very difficult due to the pressure loss limitation. When Waldron et al. (2001) carried out experiments in a 6-m-long adsorptive reactor, 88 ~ 94% purity H_2 product gas was continuously produced from the adsorptive reactor under cyclic steady-state operating conditions, where the adsorbent regeneration was carried out at subatmospheric pressure and the cyclic steady state was typically reached after 30 cycles. In our simulation, the cyclic steady state is achieved after 15 cycles, since a longer total cyclic time is used.

Conclusions

It is found that where the adsorbent and catalyst are packed in a multifunctional reactor, the methane conversion is enhanced; a high-purity hydrogen product gas with traces of CO_2 and CO can be produced at a lower temperature and lower pressure compared with the conventional steam-reforming method if the operation times are controlled. For a given system (the adsorbent, temperature, and pressure are specified), increasing the packing density, the adsorbent/catalyst ratio, and the residence time in the adsorptive reactor can improve the methane conversion, and favor the production of high-purity hydrogen.

The simulated results are in reasonable agreement with experimental data from the literature (Hufton et al., 1999; Ding and Alpay, 2000b) for sorption-enhanced steam–methane reforming. The sorption-enhanced steam–methane reforming is carried out at a high pressure ($P_H = 445.7$ kPa) and the regeneration of the adsorbent that was saturated with CO_2 is carried out at a low pressure ($P_L = 125.7$ kPa). Under the cyclic steady-state conditions, 80% average purity H_2 product gas with traces of CO_2 and CO can be continuously produced from a 2-m-long adsorptive reactor. Increasing the length of the adsorptive reactor produces a higher purity H_2 product gas, but regeneration of the adsorbent then becomes very difficult due to the pressure loss limitation. Therefore, the regeneration method needs to be improved. The total cyclic time is higher than that in the conventional pressure swing adsorptive reactor, and so the cyclic steady state is quickly reached.

Acknowledgments

One of the authors (G.-h.X.) acknowledges financial support from FCT No. SFRH/BPD/1538/2000 and POCTI/32654/EQU/2000. Prof. S. Farooq kindly provided the program for calculating the roots of the collocation points and the matrix.

Notation

A = cross-sectional area of the reactor, m^2
b_{CO_2} = Langmuir model constant for component CO_2, Pa^{-1}
C = total molar concentration in the bulk phase, mol/m^3
C_{fi} = gas-phase concentration of component i in the feed, mol/m^3
C_i = molar concentration of gas-phase component i, mol/m^3
C_{pg} = gas-phase heat capacity, $J/mol \cdot K$
C_{ps} = solid-phase heat capacity, $J/kg \cdot K$
C_{vg} = heat capacity of gas phase at constant volume, $J/mol \cdot K$
d_p = particle diameter, m
D_m = molecular diffusivity, m^2/s
D_p = combination of molecular and Knudsen diffusivity, m^2/s
D_L = axial dispersion coefficient, m^2/s
m_{CO_2} = Langmuir model constant for component CO_2, mol/kg
M = average molar weight of the gas mixture, kg/mol
n = cycle number
k_{CO_2} = LDF mass-transfer coefficient, s^{-1}
k_g = gas-phase thermal conductivity, $J/m \cdot s \cdot K$
k_i = rate constant of reaction i, $i = 1, 2$: mol $Pa^{0.5}$/kg-cat $\cdot$ s, $i = 3$: mol/kg-cat $\cdot$ s
k_p = particle thermal conductivity, $J/m \cdot s \cdot K$
k_z = effective thermal conductivity, $J/m \cdot s \cdot K$
K_D = Ergun equation coefficient, $N \cdot s/m^4$
K_V = Ergun equation coefficient, $N \cdot s^2/m^5$
L = reactor length, m
P = local total pressure, Pa
P_i = partial pressure of gas-phase component i, Pa
P_H = high pressure, Pa
P_L = low pressure, Pa
$\bar{q}_i$ = solid-phase concentration for component i (average over an adsorbent particle), mol/kg
q^* = equilibrium solid-phase concentration, mol/kg
r_i = formation or consumption rate of component i, mol/kg-cat $\cdot$ s
r_p = radius of the adsorbent, m
R = universal gas constant, $J/mol \cdot K$
R_0 = inner radius of the reactor, m
R_j = reaction rate defined by Eq. 1, mol/kg-cat $\cdot$ s
t = time, s
t_i = operational time for step i, s
T = temperature in bulk gas-phase, K
T_f = feed gas temperature, K
T_w = wall temperature, K
u = superficial velocity, m/s
u_{i0} = initial superficial velocity for step i, m/s
U = overall bed-wall heat-transfer coefficient, $J/m^2 \cdot K$
υ_{ij} = stoichiometric coefficient of component i in reaction j
y_{fi} = gas-phase mole fraction of component i in the feed
y_i = gas-phase mole fraction of component i
z = axial coordinate in bed, m

Greek letters

α = mass ratio of adsorbent and catalyst in the packed bed
ϵ_b = bed porosity
ϵ_p = adsorbent porosity
ϵ_t = total bed porosity
η_j = catalyst effectiveness factor
$\zeta = z/L$
μ = viscosity of fluid, kg/m·s
ρ_{ad} = mass of adsorbent per bed volume, kg/m^3
ρ_b = bulk packing density of the adsorbent and catalyst, kg/m^3
ρ_{cat} = mass of catalyst per bed volume, kg/m^3
ρ_g = gas-phase density, kg/m^3
ρ_p = adsorbent pellet density, kg/m^3
$-\Delta H_{adi}$ = adsorption heat of component i (on the adsorbent surface), J/mol
ΔH_{Ri} = reaction heat of reaction i, J/mol

Literature Cited

Adris, A. M., C. J. Lim, and J. R. Grace, "The Fluidized Bed Membrane Reactor System: A Pilot Scale Experimental Study," *Chem. Eng. Sci.*, **49**, 5833 (1994).

Alpay, E., C. N. Kenney, and D. M. Scott, "Simulation of Rapid Pressure Swing Adsorption and Reaction Processes," *Chem. Eng. Sci.*, **48**, 3173 (1993).

Alpay, E., D. Chatsiriwech, K. S. Kershenbaum, C. P. Hull, and N. F. Kirkby, "Combined Reaction and Separation in Pressure Swing Processes," *Chem. Eng. Sci.*, **49**, 5845 (1994).

Anand, M., J. Hufton, S. Mayorga, S. Nataraja, S. Sircar, and T. Gaffiney, "Sorption Enhanced Reaction (SERP) for the Production of Hydrogen," APCI Report for DOE, DOE, Washington, DC (1995).

Armor, J. N., "Membrane Catalysis: Where Is It now, What Needs to Be Done?" *Catal. Today*, **25**, 199 (1995).

Balachandran, U., J. T. Dusek, P. S. Maiya, B. Ma, R. L. Mierill, M. S. Kleefisil, and C. A. Udovich, "Ceramic Membrane Reactor for Converting Methane to Syngas," *Catal. Today*, **36**, 265 (1997).

Bird, R. B., W. E. Stewart, and E. N. Lightfoot, *Transport Phenomena*, Wiley, New York (1960).

Carvill, B. T., J. R. Hufton, M. Anand, and S. Sircar, "Sorption-Enhanced Reaction Process," *AIChE J.*, **42**, 2765 (1996).

Champagnie, A. M., T. T. Tsotsis, R. G. Minet, and I. A. Webster, "High Temperature Catalytic Membrane Reactor for Ethane Dehydrogenation," *Chem. Eng. Sci.*, **45**, 2423 (1990).

Chatsiriwech, D., E. Alpay, L. S. Kershenbaum, C. P. Hull, and N. F. Kirkby, "Enhancement of Catalytic Reaction by Pressure Swing Adsorption," *Catal. Today*, **20**, 351 (1994).

Cho, B. K., R. Aris, and R. W. Carr, "A Continuous Chromatographic Reactor," *Chem. Eng. Sci.*, **35**, 74 (1980).

Cho, B. K., R. Aris, and R. W. Carr, "The Mathematical Theory of a Countercurrent Chromatographic Reactor," *Proc. R. Soc. (London)*, **A38**, 147 (1982).

Chu, C., and L. C. Tsang, "Behavior of Chromatographic Reactor," *Ind. Eng. Chem. Process Des. Dev.*, **10**, 47 (1971).

Da Silva, F. A., and A. E. Rodrigues, "Propylene/Propane Separation by Vacuum Swing Adsorption Using 13X Zeolite," *AIChE J.*, **47**, 341 (2001).

De Wash, A. P., and G. F. Froment, "Heat Transfer in Packed Bed," *Chem. Eng. Sci.*, **27**, 567 (1972).

Ding, Y., and E. Alpay, "Equilibria and Kinetics of CO_2 Adsorption on Hydrotalcite Adsorbent," *Chem. Eng. Sci.*, **55**, 3461 (2000a).

Ding, Y., and E. Alpay, "Adsorption-Enhanced Steam-Methane Reforming," *Chem. Eng. Sci.*, **55**, 3929 (2000b).

Edwards, M. F., and J. F. Richardson, "Gas Dispersion in Packed Beds," *Chem. Eng. Sci.*, **23**, 109 (1968).

Ergun, S., "Fluid Flow Through Packed Columns," *Chem. Eng. Prog.*, **48**, 89 (1952).

Fish, B., R. W. Carr, and R. Aris, "The Continuous Countercurrent Moving Bed Chromatographic Reactor," *Chem. Eng. Sci.*, **41**, 661 (1986).

Gluud, W., K. Keller, R. Schonfelder, and W. Klempt, "Production of Hydrogen," U. S. Patent No. 1,816,523 (1931).

Han, C., and D. P. Harrison, "Simultaneous Shift Reaction and Carbon Dioxide Separation for the Direct Production of Hydrogen," *Chem. Eng. Sci.*, **49**, 5875 (1994).

Hayhurst, D. T., "Gas Adsorption by Some Natural Zeolites," *Chem. Eng. Commun.*, **4**, 729 (1980).

Hsieh, H. P., "Inorganic Membrane Reactors—A Review," *AIChE Symp. Ser.*, **85**, 53 (1989).

Hufton, J. R., S. Mayorga, and S. Sircar, "Sorption-Enhanced Reaction Process for Hydrogen Production," *AIChE J.*, **45**, 248 (1999).

Hufton, J. R., W. Waldron, S. Weigel, M. Rao, and S. Sircar, "Sorption Enhanced Reaction Process (SERP) for the Production of Hydrogen," *Proc. U.S. DOE Hydrogen Program Rev.*, **1**, 70 (2000).

Itoh, N., W. C. Xu, and A. M. Sathe, "Capability of Permeate Hydrogen through Palladium-Based Membranes for Acetylene Hydrogenation," *Ind. Eng. Chem. Res.*, **32**, 2614 (1993).

Jachuck, R. J. J., and C. Ramshaw, "Process Intensification: Polymer Film Compact Heat Exchanger (PFCHE)," *Chem. Eng. Res. Des.*, **72**, 255 (1994).

Kikkinides, E. S., R. T. Yang, and S. H. Cho, "Concentration and Recovery of CO_2 from Flue Gas by Pressure Swing Adsorption," *Ind. Eng. Chem. Res.*, **32**, 2714 (1993).

Kirkby, N. F., and J. E. P. Morgan, "A Theoretical Investigation of Pressure Swing Reaction," *Trans. Inst. Chem. Eng.*, **72**, 541 (1994).

Kruglov, A. V., "Methanol Synthesis in a Simulated Countercurrent Moving Bed Adsorptive Catalytic Reactor," *Chem. Eng. Sci.*, **49**, 4699 (1994).

Lee, I. D., and R. H. Kadlec, "Effects of Adsorbent and Catalyst Distributions in Pressure Swing Reactors," *AIChE Symp. Ser.*, **84**, 167 (1989).

Li, C. H., and B. A. Finlayson, "Heat Transfer in Packed Bed—A Reevaluation," *Chem. Eng. Sci.*, **32**, 1055 (1977).

Lu, Z. P., and A. E. Rodrigues, "Pressure Swing Adsorption Reactors: Simulation of Three-Step One-Bed Process," *AIChE J.*, **40**, 1118 (1994).

Ma, Y. H., and C. Mancel, "Diffusion Studies of CO_2, NO, NO_2, and SO_2 on Molecular Sieve Zeolites by Gas Chromatography," *AIChE J.*, **18**, 1148 (1972).

Ma, Y. H., and A. J. Roux, "Multicomponent Rates of Sorption of SO_2 and CO_2 in Sodium Mordenite," *AIChE J.*, **19**, 1055 (1973).

Magee, E. M., "The Course of a Reaction in a Chromatographic Column," *Ind. Eng. Chem. Fundam.*, **2**, 32 (1963).

Malek, A., and S. Farooq, "Study of a Six-Bed Pressure Swing Adsorption Process," *AIChE J.*, **43**, 2509 (1997).

Matros, Y. Sh., and G. A. Bunimovich, "Control of Volatile Organic Compounds by the Catalytic Reverse Process," *Ind. Eng. Chem. Res.*, **34**, 1630 (1995).

Omorjan, R. P., R. N. Paunovis, and M. N. Tekic, "Applicability of a Double-Membrane Reactor for Thermal Decomposition of Water: A Computer Analysis," *J. Membr. Sci.*, **154**, 273 (1999).

Ostrowski, T., and L. Mleczko, "Simulations of the Effect of Hydrodynamic Conditions and Properties of Membranes on the Catalytic Performance of a Fluidized-Bed Membrane Reactor for Partial Oxidation of Methane," *Can. J. Chem. Eng.*, **77**, 363 (1999).

Petroulas, T., R. Aris, and R. W. Carr, "Analysis and Performance of a Countercurrent Moving Bed Chromatographic Reactor," *Chem. Eng. Sci.*, **40**, 2233 (1985).

Reid, R. C., J. M. Prausnitz, and B. E. Poling, *The Properties of Gases and Liquids*, McGraw-Hill, New York (1988).

Ridler, D. E., and M. V. Twigg, "Steam Reforming," *Catalyst Handbook*, Wolfe, London, p. 225 (1989).

Roginskii, S. Z., M. J. Yanovskii, and G. A. Graziev, "Catalytic Reactions and Catalysis under Chromatographic Reactor," *Kinet. Katal.*, **3**, 529 (1962).

Rostrup-Nielsen, J. R., "Industrial Catalysis, the Science and the Challenge. Conversion of Fossil Fuels," *Catal. Today*, **18**, 125 (1993).

Salinger, A. G., and G. Eigenberger, "Direct Calculation of Periodic States of the Reverse Flow Reactor. I. Methodology and Propane Combustion Results," *Chem. Eng. Sci.*, **51**, 4903 (1996).

Sereno, C., and A. E. Rodrigues, "Can Steady-State Momentum Equations Be Used in Modeling Pressurization of Adsorption Beds?" *Gas Sep. Purif.*, **7**, 167 (1993).

Silva, J. A. C., and A. E. Rodrigues, "Separation of *n*/iso-Paraffins Mixtures by Pressure Swing Adsorption," *Sep. Purif. Technol.*, **13**, 195 (1998).

Sun, Y. M., and S. J. Khang, "Catalytic Membrane for Simultaneous Chemical Reaction and Separation Applied to a Dehydrogenation Reaction," *Ind. Eng. Chem. Res.*, **27**, 1136 (1988).
Takeuchi, K., and Y. Uraguchi, "Experimental Studies of a Chromatographic Moving Bed Reactor," *J. Chem. Eng. Jpn.*, **10**, 455 (1977).
Tonkovich, A. L. Y., and R. W. Carr, "A Simulated Countercurrent Moving Bed Chromatographic Reactor for the Oxidative Coupling of Methane: Experimental Results," *Chem. Eng. Sci.*, **49**, 4647 (1994a).
Tonkovich, A. L. Y., and R. W. Carr, "Modelling of the Simulated Countercurrent Moving Bed Reactor Used for the Oxidative Coupling of Methane," *Chem. Eng. Sci.*, **49**, 4657 (1994b).
Tsotsis, T. T., A. M. Champagnie, S. P. Vasileiadis, Z. D. Zraka, and R. G. Minet, "Packed Bed Catalytic Membrane Reactor," *Chem. Eng. Sci.*, **47**, 2903 (1992).
Twigg, M. V., *Catalyst Handbook*, Wolfe, London (1989).
Uemiya, S., N. Sato, H. Ando, and E. Kikuchi, "The Water Gas Shift Reaction Assisted by a Palladium Membrane Reactor," *Ind. Eng. Chem. Res.*, **30**, 585 (1991).
Valenzuela, D. P., and A. L. Myers, *Adsorption Equilibrium Data Handbook*, Prentice Hall, Englewood Cliffs, NJ, p. 39 (1989).
Vaporciyan, G. G., and R. H. Kadlec, "Equilibrium Limited Periodic Separating Reactors," *AIChE J.*, **33**, 1334 (1987).
Vaporciyan, G. G., and R. H. Kadlec, "Periodic Separating Reactors: Experiments and Theory," *AIChE J.*, **35**, 831 (1989).
Waldron, W. E., J. R. Hufton, and S. Sircar, "Production of Hydrogen by Cyclic Sorption Enhanced Reaction Process," *AIChE J.*, **47**, 1477 (2001).
Wilson, R. J., and R. P. Danner, "Adsorption of Synthesised Gas-Mixture Components on Activated Carbon," *J. Chem. Eng. Data*, **28**, 14 (1983).
Wu, J. C. S., T. E. Gerdes, J. L. Pszczolowski, R. Bhave, and P. K. T. Liu, "Dehydrogenation of Ethylbenzene to Styrene Using Commercial Ceramic Membranes as Reactors," *Sep. Sci. Technol.*, **25**, 1489 (1990).
Xiu, G. H., P. Li, and A. E. Rodrigues, "Sorption-Enhanced Reaction Process with Intraparticle Diffusion Limitation," *Proc. Int. Symp. on Chemical Reaction Engineering*, Hong Kong (2002).
Xu, J., and G. F. Froment, "Methane Steam Reforming, Methanation and Water-Gas Shift: 1. Intrinsic Kinetics," *AIChE J.*, **35**, 89 (1989).
Yagi, S., D. Kunii, and N. Wakao, "Studies on Axial Effective Thermal Conductivities in Packed Beds," *AIChE J.*, **6**, 543 (1960).
Yongsunthon, I., and E. Alpay, "Conversion-Temperature Trajectories for Well-Mixed Adsorptive Reactors," *Chem. Eng. Sci.*, **53**, 691 (1998).
Yongsunthon, I., and E. Alpay, "Design of Periodic Adsorptive Reactors for the Optimal Integration of Reaction, Separation and Heat Exchange," *Chem. Eng. Sci.*, **54**, 2647 (1999).
Zou, Y., V. Mata, and A. E. Rodrigues, "Adsorption of Carbon Dioxide onto Hydrotalcite-Like Compounds (HTLCs) at High Temperatures," *Ind. Eng. Chem. Res.*, **40**, 204 (2001).

Manuscript received Dec. 12, 2001, and revision received Jun. 28, 2002.